photomicroscopy were conducted with an Olympus BX50 and a Wild M400 Photomakroskop. Images were captured with a Spot RT slider digital camera (Diagnostic Instruments), and image files were processed with Photoshop (Adobe) and Canvas (Deneba) software. Images for publication were corrected for contrast and brightness.

Received 19 February; accepted 23 April 2003; doi:10.1038/nature01698.

1. Redgrave, P., Prescott, T. J. & Gurney, K. The basal ganglia: a vertebrate solution to the selection problem. *Neuroscience* **89,** 1009–1023 (1999).
2. Stein, B. E. & Meredith, M. A. *The Merging of the Senses* (MIT Press, Cambridge, Massachusetts, 1993).
3. Lee, C., Rohrer, W. H. & Sparks, D. L. Population coding of saccadic eye movements by neurons in the superior colliculus. *Nature* **332,** 357–360 (1988).
4. Munoz, D. P. & Guitton, D. Tectospinal neurons in the cat have discharges coding gaze position error. *Brain Res.* **341,** 184–188 (1985).
5. Chevalier, G., Vacher, S. & Deniau, J. M. Inhibitory nigral influence on tectospinal neurons, a possible implication of basal ganglia in orienting behaviour. *Exp. Brain Res.* **53,** 320–326 (1984).
6. Chevalier, G., Vacher, S., Deniau, J. M. & Desban, M. Disinhibition as a basic process in the expression of striatal function. I. The striato-nigral influence on tecto-spinal/tecto-diencephalic neurons. *Brain Res.* **334,** 215–226 (1985).
7. Hikosaka, O. & Wurtz, R. H. Visual and oculomotor function of monkey substantia nigra pars reticulata. IV. Relation of substantia nigra to superior colliculus. *J. Neurophysiol.* **49,** 1285–1301 (1983).
8. Joseph, J. P. & Boussaoud, D. Role of the cat substantia nigra pars reticulata in eye and head movements. 1. Neural activity. *Exp. Brain Res.* **57,** 286–296 (1985).
9. Beckstead, R. M. A comparison of the intranigral disribution of nigrotectal neurons labelled with horseradish peroxidase in the monkey, cat and rat. *J. Neurosci.* **1,** 121–125 (1981).
10. Harting, J. K., Huerta, M. F., Hashikawa, R., Weber, J. T. & Van Lieshout, D. P. Neuroanatomical studies of the nigrotectal projection in the cat. *J. Comp. Neurol.* **278,** 615–631 (1988).
11. Chevalier, G., Thierry, A. M., Shibazaki, T. & Feger, J. Evidence for a GABAergic inhibitory nigrotectal pathway in the rat. *Neurosci. Lett.* **21,** 67–70 (1981).
12. Karabelas, A. B. & Moschovakis, A. K. Nigral inhibitory termination of efferent neurons of the superior colliculus: an intracellar horseradish peroxidase study in the cat. *J. Comp. Neurol.* **239,** 309–329 (1985).
13. May, P. J. & Hall, W. C. Relationships between the nigrotectal pathway and the cells of origin of the predorsal bundle. *J. Comp. Neurol.* **226,** 357–376 (1984).
14. Chevalier, G. & Deniau, J. M. Disinhibition as a basic process in the expression of striatal functions. *Trends Neurosci.* **13,** 277–280 (1990).
15. Wallace, S. F., Rosenquist, A. C. & Sprague, J. M. Ibotenic acid lesions of the lateral substantia nigra restore visual orientation behaviour in the hemianopic cat. *J. Comp. Neurol.* **296,** 222–252 (1990).
16. Ryan, L. J. & Clark, K. B. The role of the subthalamic nucleus in the response of globus pallidus neurons to stimulation of the prelimbic and agranular frontal cortices in rats. *Exp. Brain Res.* **86,** 641–651 (1991).
17. Kha, H. T. *et al.* Projections from the substantia nigra pars reticulata to the motor thalamus of the rat: single axon reconstructions and immunohistochemical study. *J. Comp. Neurol.* **440,** 20–30 (2001).
18. Mize, R. R., Luo, Q., Butler, G., Jeon, C. J. & Nabors, B. The calcium-binding proteins parvalbumin and calbindin-D 28K form complementary patterns in the cat superior colliculus. *J. Comp. Neurol.* **320,** 243–256 (1992).
19. Kalesnykas, R. P. & Sparks, D. L. The interaction of visual and electrical activity of neurons in the monkey superior colliculus: Site and train characteristics affect saccade latency, amplitude and direction. *Soc. Neurosci. Abstr.* **25,** 1920 (1999).
20. Wang, S. & Redgrave, P. Microinjections of muscimol into lateral superior colliculus disrupt orienting and oral movements in the formalin model of pain. *Neuroscience* **81,** 967–988 (1997).
21. Infante, C. & Leiva, J. Simultaneous unitary neuronal activity in both superior colliculi and its relation to eye movements in the cat. *Brain Res.* **381,** 390–392 (1986).
22. Behan, M. An EM-autoradiographic and EM-HRP study of the commissural projection of the superior colliculus in the cat. *J. Comp. Neurol.* **234,** 105–116 (1985).
23. Mink, J. W. The basal ganglia: focused selection and inhibition of competing motor programs. *Prog. Neurobiol.* **50,** 381–425 (1996).
24. Handel, A. & Glimcher, P. W. Contextual modulation of substantia nigra pars reticulata neurons. *J. Neurophysiol.* **83,** 3042–3048 (2000).
25. Sato, M. & Hikosaka, O. Role of primate substantia nigra pars reticulata in reward-oriented saccadic eye movement. *J. Neurosci.* **22,** 2363–2373 (2002).
26. Alexander, G. E. & Crutcher, M. D. Functional architecture of basal ganglia circuits: neural substrates of parallel processing. *Trends Neurosci.* **13,** 266–271 (1990).
27. Kita, H. & Kitai, S. T. Efferent projections of the subthalamic nucleus in the rat: light and electron microscopic analysis with the PHA-L method. *J. Comp. Neurol.* **260,** 435–452 (1987).
28. Sprague, J. M. Interactions of cortex and superior colliculus in mediation of visually guided behavior in the cat. *Science* **153,** 1544–1547 (1966).
29. Wallace, S. F., Rosenquist, A. C. & Sprague, J. M. Recovery from cortical blindness mediated by destruction of nontectotectal fibres in the commissure of the superior colliculus in the cat. *J. Comp. Neurol.* **284,** 429–450 (1989).
30. Karnath, H. O. New insights into the functions of the superior temporal cortex. *Nature Rev. Neurosci.* **2,** 568–576 (2001).

Acknowledgements We thank R. Coghill, P. Redgrave and T. Stanford for their critical comments on earlier versions of the manuscript, and N. London for editorial assistance. This work was supported by a grant from the National Institutes of Health to J.G.M. H.J. was partly supported by a grant from the National Institutes of Health to B.E.S.

Competing interests statement The authors declare that they have no competing financial interests.

Correspondence and requests for materials should be addressed to J.G.M. (mchaffie@wfubmc.edu).

Mapping multiple features in the population response of visual cortex

Amit Basole*, Leonard E. White*† & David Fitzpatrick*

** Department of Neurobiology and † Department of Community and Family Medicine, Duke University Medical Center, Durham, North Carolina 27710, USA*

Stimulus features such as edge orientation, motion direction and spatial frequency are thought to be encoded in the primary visual cortex by overlapping feature maps arranged so that the location of neurons activated by a particular combination of stimulus features can be predicted from the intersections of these maps[1–8]. This view is based on the use of grating stimuli, which limit the range of stimulus combinations that can be examined. We used optical imaging of intrinsic signals[9] in ferrets to assess patterns of population activity evoked by the motion of a texture (a field of iso-oriented bars). Here we show that the same neural population can be activated by multiple combinations of orientation, length, motion axis and speed. Rather than reflecting the intersection of multiple maps, our results indicate that population activity in primary visual cortex is better described as a single map of spatiotemporal energy.

Orderly relationships between overlapping feature maps in the visual cortex are thought to ensure that all combinations of stimulus features are represented uniformly across the visual field[2–8]. In this conception, a specific combination of stimulus features (such as a vertical stimulus of high spatial frequency moving to the right) is represented by a unique pattern of population activity that corresponds to appropriate intersecting regions of different feature maps. This view is based on the analysis of cortical responses to drifting gratings in which the range of motion and spatial frequency cues is limited to those that vary along an axis orthogonal to the grating's orientation[10–12]. As a result, it has not been possible to examine interactions between motion, orientation and spatial frequency that are common in the visual environment. To decouple these stimulus features, we used texture stimuli composed of iso-oriented line segments[13,14] (see Supplementary Fig. 1a). Patterns of cortical activity evoked by various combinations of line orientation and axis of motion were assessed by optical imaging of intrinsic signals and by electrophysiological recordings; in addition we explored how these patterns were altered by changes in line length and motion speed.

Texture stimuli produced strong and reliable activation of visual cortical neurons, evoking a spatial pattern whose structure and periodicity resembled that found with square-wave grating stimuli (Fig. 1). For texture stimuli moved along axes perpendicular to the line elements, the activation patterns were statistically indistinguishable from those evoked by gratings of the same orientation (Fig. 1a–c). For example, a 45° texture yielded a population response (Fig. 1c; see Methods) that peaked near 45° and was similar to that found for a 45° grating. Across the seven animals examined, the peak and width of the population response for textures with orthogonal motion (peak = 42° ± 3° (mean ± s.e.m.), half-width at half-height = 46.7° ± 3.6°) were not significantly different from that for gratings (peak = 41° ± 1°, half-width = 40° ± 2.3°; $P = 0.7$ and 0.1 respectively, t-test). The tuning functions derived from the optical responses were also well fitted by gaussian functions (average R^2 for gratings = 0.91 ± 0.02; for textures $R^2 = 0.90 \pm 0.03$).

In contrast, movement of the textures along non-orthogonal axes produced population responses that differed significantly from those found in response to gratings matching the orientation of the texture bars. For example, a 45° clockwise shift in the axis of motion, without altering the orientation of the line elements (45°),

changed the distribution of population activity so that it peaked near 20° rather than 45° (Fig. 1f). This shift can also be appreciated qualitatively in the difference images (compare Fig. 1a and d). In a symmetrical fashion, a 45° anticlockwise shift in the axis of motion changed the population response such that its peak was at 75° (Fig. 1i; compare Fig. 1a and 1g). Despite the fact that the images in Fig. 1d, g were obtained with textures consisting of 45° bars, the activity patterns were very different from each other ($R^2 = 0.01$; see Methods), indicating a strong effect of axis of motion. Across the seven animals examined, a 45° offset between the orientation of the elements and the axis of motion yielded an average shift in the peak of the population response of 39° (±3°). Correspondingly smaller shifts in the peak of the population response were found for a 22.5° offset in the axis of motion (20° ± 7°).

Despite these shifts, the pattern of population activity for non-orthogonal motion still resembled that found with grating stimuli. The average half-width of the population response for textures moving non-orthogonally was quite similar to the orthogonal texture or the grating response (39.1° ± 2.7°), as was the average R^2 value for the best-fit gaussian function (0.94 ± 0.02). However, the patterns were now more similar to those evoked by gratings whose orientation differed from the orientation of the texture elements. For Fig. 1d–f the pattern resembled that evoked by a more acute grating angle ($R^2 = 0.46$ between difference images in Fig. 1d and e), whereas for Fig. 1g–i it resembled that evoked by a less acute grating angle ($R^2 = 0.7$ between difference images in Fig. 1g, h). In both cases the patterns are quite different from those evoked by an orientation-matched grating ($R^2 = 0.25$ between difference images in Fig. 1d and b and 0.16 between difference images in Fig. 1g and b). These results suggest that the iterated pattern of activity resulting from the presentation of a grating stimulus, which has been thought to represent the orientation of the grating, can be elicited by a range of different orientation and axis-of-motion combinations made possible by the use of texture stimuli (see Supplementary Fig. 1b).

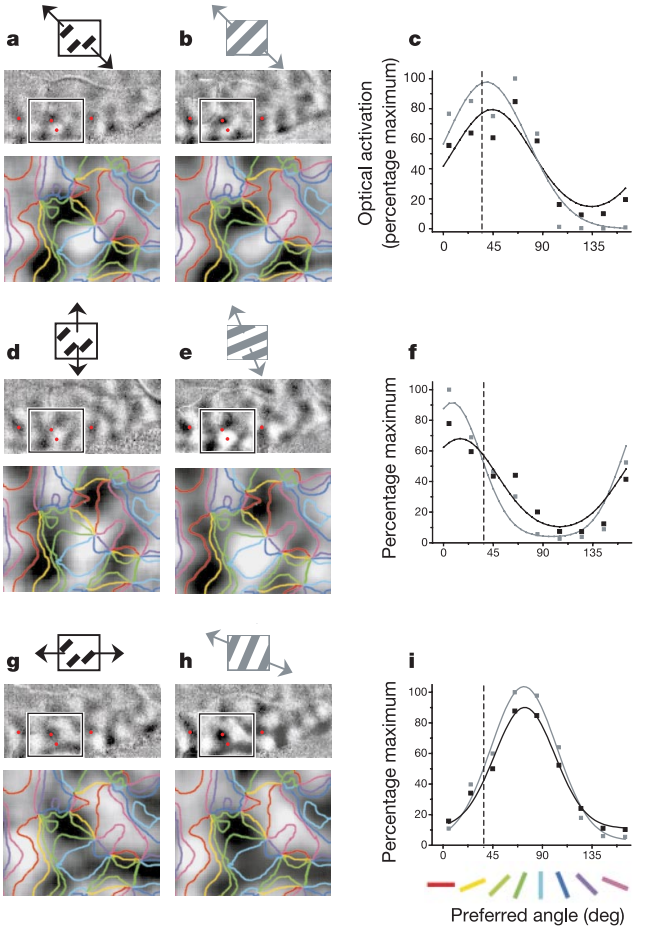

Figure 1 Systematic shifts in the population response induced by changes in axis of motion. Each panel contains texture (**a**, **d**, **g**) or grating (**b**, **e**, **h**) difference images, with insets showing iso-orientation contours derived from the grating angle map overlaid on the boxed region of interest (see angle colour key below graph, inset width = 1.7 mm). The red dots are placed over identical regions of each image to facilitate comparison. Graphs quantify the population response (**c**, **f**, **i**: black curve, texture response; grey curve, grating response). The dashed vertical line is placed at the same position on the *x*-axis to compare the relative shift between the curves. **a**–**c**, Orthogonally moving textures and gratings of the same orientation evoke similar responses. **d**–**f**, A 45° clockwise shift in texture motion evokes a response similar to a 22° grating. **g**–**i**, A 45° anticlockwise shift in texture motion evokes a response similar to a 67° grating.

The dissociation of the activity patterns for textures from patterns evoked by their orientation-matched gratings is further emphasized under conditions in which the length of the texture line segments is altered without changing either the line orientation or the axis of motion. All experiments shown in Fig. 1 were performed by keeping the bar length fixed at 6° of visual angle. Increasing the line length from 2° to 10° without changing the line orientation (45°) or the axis of motion (horizontal) produced a systematic change in the population response (Fig. 2a and Supplementary movie 1). Quantification of the population response shows the progressive shift in the peak with increasing stimulus length, from a peak of 87° for short line segments to 56° for long line segments. Similar results were obtained in all eight animals tested (Fig. 2c). The average change in the peak with change in line length from 2° to 10° was 31° and this difference was highly significant ($P < 0.001$, one-way analysis of variance). Because changing the line length changes the spatial frequency characteristics of the stimulus (see ref. 12), it is possible that these shifts in the pattern of population activity could be attributable to the orderly mapping of spatial frequency[5,6,15]. However, if this were so, similar changes in the population response to a change in line length should be found for a motion of the texture along the axis orthogonal to the orientation of the elements. Although increasing the line length affected the magnitude of the population response, there was no systematic change in the peak of the response for orthogonal motion (Fig. 2b). This result also excludes the possibility that the shifts in the distribution of population activity with line length can be explained by a systematic mapping of length preference such as might result from variations in length summation properties or end-stopping[16,17].

From the results presented so far, one could infer that a given pattern of activity can be elicited by a range of stimuli that are composed of different combinations of line orientation, axis of motion and length. The population response to texture stimuli therefore cannot encode a unique combination of stimulus features, nor can it simply correspond to the intersection of multiple feature maps. Instead, a description of the population response in terms of the tuning of individual neurons to a restricted range of spatial (along two dimensions) and temporal frequencies[12,18–21] might be a more appropriate framework for interpreting these results. The short line segments of the texture stimuli possess energy at many orientations in the Fourier domain[18,22] (that is, they are characterized by a broad spatial frequency spectrum). Modulation of the neural response to all Fourier components could explain why the tuning of the population response does not match that predicted from the orientation of the texture elements[21]. When the stimulus moves, each Fourier component moves at a different speed depending on its orientation relative to the direction of motion of the stimulus (see Supplementary Fig. 2). The component whose speed is optimal given the temporal tuning properties of neurons in the primary visual cortex (V1) determines the peak of the active population. Thus, a strong test of the ability of spatiotemporal

frequency tuning to account for the population response is whether the activity patterns evoked by texture stimuli are sensitive to the speed of texture motion[23,24] (but see ref. 25).

This prediction was tested by using a texture composed of 45° oriented bars of 4° length moving horizontally at 10° s^{-1}, 50° s^{-1} and 100° s^{-1}. Changes in speed resulted in significant shifts in the locus of activity (Fig. 3a). These changes correspond to a shift in the

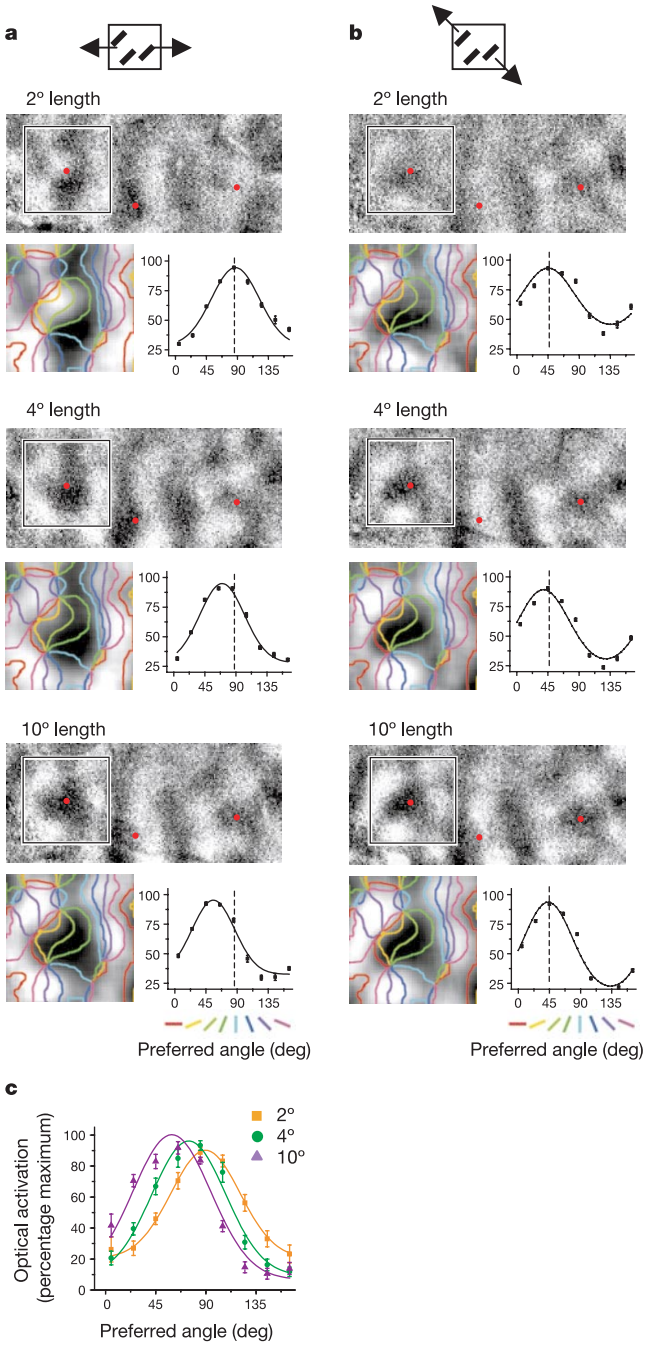

Figure 2 Systematic shifts in the population response induced by changes in bar length. **a**, Difference images, contour overlays (inset width = 1.2 mm) and population response profiles for texture stimuli of three lengths (2°, 4° and 10°) moved non-orthogonally. Increasing the bar length shifted the activity pattern and the peak of the response from 87° to 70° to 56° (from blue contours to green–yellow contours; see Supplementary movie 1). **b**, Lack of shifts with orthogonal motion. **c**, Summary of length-induced shifts with non-orthogonal textures (n = 8 animals; results are means ± s.e.m.); peaks for 2°, 4° and 10° lengths are 90°, 74° and 59°, respectively.

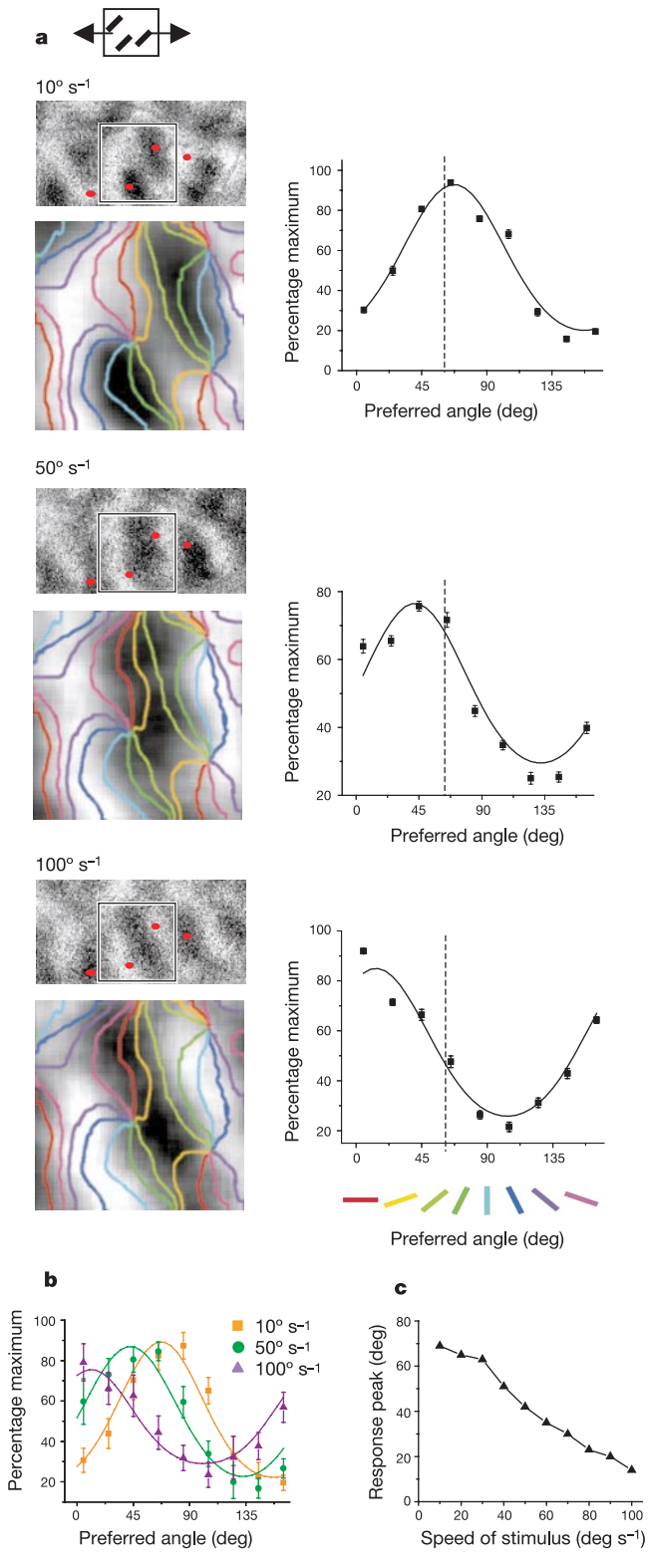

Figure 3 Shifts in the population response induced by changes in stimulus speed. **a**, Difference images, contour overlays (inset width = 1.3 mm) and population response profiles obtained with 45° texture stimuli moving horizontally at three speeds: 10° s^{-1} (peak = 69°), 50° s^{-1} (peak = 42°) and 100° s^{-1} (peak = 14°). **b**, Average population responses (means ± s.e.m.) for three speeds (n = 7 animals); the peak shifts from 73° at low speed to 47° at intermediate speed to 17° at high speed. **c**, Peaks of the population responses obtained with 10 different speeds (10–100° s^{-1} at 10° s^{-1} intervals; see Supplementary Fig. 3).

peak of the population response of 55° as the speed increased from $10° s^{-1}$ to $100° s^{-1}$. Similar results were found for all seven animals tested (Fig. 3b, change in peak with speed was significant at $P < 0.001$, one-way analysis of variance). In one animal we examined the population response to 10 speeds ranging from $10° s^{-1}$ to $100° s^{-1}$ at 10° intervals (see Supplementary Fig. 3 and Supplementary movie 2). The peak of the response varied linearly over a 60° range as speed increased (Fig. 3c; R^2 of linear fit = 0.99).

If these changes in population activity resulted from the orderly mapping of preferences for speed or temporal frequency[15,26], similar shifts should be found with grating stimuli. This did not occur (Supplementary Fig. 4a, c). The average peaks of response for vertical gratings drifting at $20° s^{-1}$ (90.3° ± 0.7°) and at $100° s^{-1}$ (89.7° ± 1°) were not significantly different ($P = 0.6$, *t*-test, $n = 6$ animals). In contrast, and consistent with the spatiotemporal energy framework, patterns of population activity induced by drifting random-dot stimuli showed pronounced changes with speed (Supplementary Fig. 4b_1, b_2, d), the average shift in peak of the population response from low to high speed, for eight animals, was 89.2° ± 4.2°. Furthermore, speed-induced changes in population response to the textures described above varied systematically with line length. Because an increase in line length narrows the power spectrum of the stimulus[21], it is predicted that the magnitude of the speed-induced shift will decrease with an increase in length. In two cases, for texture stimuli 2° long, the average shift in population tuning with change in speed from $10° s^{-1}$ to $100° s^{-1}$ was 86° ± 1.75°, for 4° textures it was 57° ± 2.7° and for 10° textures the shift was only 22° ± 8.15°.

If tuning to spatiotemporal frequency explains the population response, the activity of single neurons should display length- and speed-dependent shifts comparable to those seen with optical imaging. Shifts in the tuning of single and multiple units elicited by the same texture and dot stimuli that were used for imaging analysis were similar in magnitude and direction to those found in the population response (Fig. 4). For example, changing the length of the line segments in textures undergoing non-orthogonal motion produced significant shifts in the preferred angle of stimulus motion (Fig. 4a, b). Moreover, similar shifts were obtained with single bars moving non-orthogonally, showing that the effect did not depend on the use of texture stimuli (Supplementary Fig. 5). Changing the speed of motion of dots (Fig. 4c, d) and textures (Fig. 4e, f) also produced consistent and significant shifts in the preferred direction of stimulus motion for single units in V1. Similar shifts were observed for both direction-tuned and non-direction-tuned neurons.

These results are difficult to reconcile with the view that V1 comprises multiple maps of orientation, direction and spatial frequency whose intersections signal the presence of particular feature combinations[2–8]. Our data show that the spatial distribution of active cortical columns does not by itself specify the exact combination of stimulus features present in the scene, because many different combinations activate similar populations of neurons. Nevertheless, the spatial pattern of population activity is very sensitive to small changes in each of the properties that were tested and these changes are highly reproducible: a particular change in stimulus configuration produced similar shifts in population activity across all animals in our sample. These results indicate that the columnar architecture of V1 represents a spatiotemporal transform in which multiple features are combined. Rather than multiple maps of different stimulus features, we suggest that the mapping of one property—orientation in space-time[27,28]—accounts for both the orderly shifts in patterns of activity and the conflation of different stimulus features in the population response. □

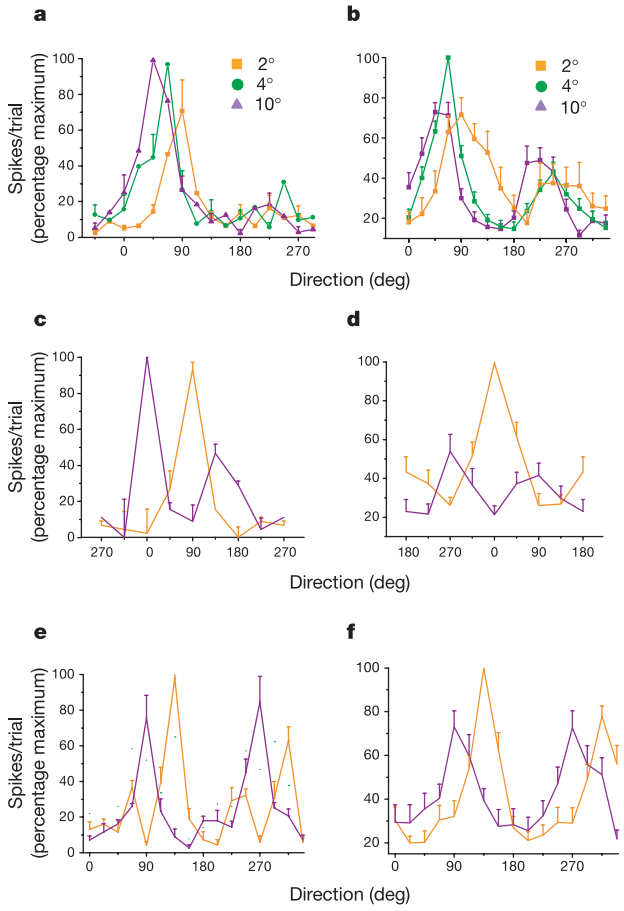

Figure 4 Tuning shifts seen with imaging occur at the single unit level. **a**, Tuning curves for a single unit obtained with non-orthogonally moving textures. The preferred angle shifts as the bar length increases. **b**, Average tuning curves for all recorded units for three stimulus lengths ($n = 11$ units for 2° length, 23 units for 4° length and 20 units for 10° length). **c**, Tuning curves for a single unit obtained with random-dot patterns drifting at $20° s^{-1}$ (orange line) and $100° s^{-1}$ (violet line). **d**, Average tuning curves obtained with random dots for the same two speeds ($n = 13$ units). **e**, Tuning curves for a single unit obtained with non-orthogonally moving textures drifting at $20° s^{-1}$ and $100° s^{-1}$. **f**, Average tuning curves obtained with non-orthogonally moving textures at the same two speeds ($n = 13$ units). All results are means and s.e.m.

Methods

Ethical approval

All experimental procedures were approved by the Duke University Institutional Animal Care and Use Committee and were performed in compliance with guidelines published by the National Institutes of Health (USA).

Surgical procedures

Animals were prepared for optical imaging as described in ref. 29. In brief, ferrets (postnatal days 45–65) were anaesthetized with a mixture of ketamine and xylazine. A hole was made in the cranium over the visual cortex, the dura was reflected and a chamber made of agar and a glass coverslip was mounted over the brain. Ferrets were paralysed with rocuronium bromide ($0.3 mg kg^{-1} h^{-1}$) either intraperitoneally or intravenously and respirated with a mixture of N_2O:O_2 (2:1) supplemented with 0.5–1.5% halothane. Expired CO_2 was maintained at 4% and body temperature was maintained at 37 °C.

Optical imaging and visual stimulation

Optical imaging of intrinsic signals was performed with an enhanced video acquisition system (Optical Imaging) as described previously[9,29]. Stimuli were full-field (80° × 60°) high-contrast square-wave gratings, full-field textures, coherently drifting random-dot patterns or single bars. Dots were 0.25° in diameter with a density of ~10 dots per 10 square degrees. Textures were pseudo-randomly placed high-contrast square-wave bars whose length, width, density and orientation could be varied. Bar density was decreased while increasing the length to control for total luminance. Bar width was always 1° while length was varied as described above. Difference images were generated by subtracting the optical responses to the presentation of a particular orientation or axis of motion from its orthogonal angle or axis. Thus, a 90° grating image was produced by subtracting the

response to a 90° grating from that to a 0° grating. For stimuli undergoing non-orthogonal motion, both the orientation and the axis of motion were different by 90° between the subtracted stimuli. For example, the response to a texture with 45° oriented bars moving horizontally was subtracted from the response to a texture with 135° oriented bars moving vertically. Results obtained with difference imaging were verified with single-condition imaging by subtracting the response to a blank screen from the stimulus-driven response (see Supplementary Fig. 6).

Optical map analysis

To interpret the patterns of activity evoked by various stimulus configurations, we developed a population response profile that captured the relative activation of each pixel in the region of interest and expressed these values in terms of the pixel's preferred orientation assessed with gratings. Grating images obtained for four to eight orientations were low-pass and high-pass filtered and vector-summed to produce referent grating-angle maps[9]. To compute a population response profile for a given stimulus, the difference image for that stimulus was assigned a threshold at the mean grey value and each pixel above the threshold was weighted (greyscale value minus threshold). On the basis of each pixel's preferred grating orientation, the weighted pixel values were summed into nine 20° angle bins (from 0° to 180°) and normalized to the highest count across conditions (for example, across length or speed). The resulting histograms were fitted with gaussian functions and the peak and width of the response were determined along with the R^2 value of the best-fit gaussian function. For direct comparison between any two images, the two-dimensional correlation coefficient (R) between the two (high-pass and low-pass filtered) images was determined with the Matlab Image Processing Toolbox (Mathworks, Natick, Massachusetts). This value was then squared and reported as the more intuitive coefficient of determination (R^2).

Difference images shown in figures were high-pass filtered and a region of interest was selected for demonstration purposes. The region of interest was selected as the region of the image that showed both a strong response and a representative shift with change in stimulus conditions. Contour overlays were prepared by superimposing iso-orientation contours from a referent grating-angle map over a filtered and re-clipped (to ± 2 s.d.) texture, dot or grating difference image.

Electrophysiology

Single and multiple units were recorded extracellularly from V1 with a tungsten microelectrode (impedance 8–14 MΩ). Action potentials were recorded from the superficial layers (<400 μm) and discriminated by using Spike2 software (Cambridge Electronic Design, Cambridge, UK). Orientation and direction tuning functions were obtained for each site by panning a bar (40° × 0.4°) across the receptive field. Tuning curves for textures or dots were obtained by panning full-field textures (at eight orientations) or a field of dots in 16 directions (at 22.5° intervals). For non-orthogonal motion, the offset between bar orientation and direction of motion was 45°. For the single-bar experiments, the centre and size of the minimal discharge field were determined by using a small orthogonally drifting bar. A square-wave bar of varying length was then moved non-orthogonally such that it always passed through the centre of the receptive field. In some cases, 3–10 speeds were randomized within the direction tuning experiment. Action potentials were counted for the entire stimulus duration (1–2 s). Offline spike sorting and tuning analysis was performed with custom-written Spike2 software.

Received 13 January; accepted 23 April 2003; doi:10.1038/nature01721.

1. Hubel, D. H. & Wiesel, T. N. Ferrier Lecture: Functional architecture of macaque monkey visual cortex. *Proc. R. Soc. Lond. B* **198,** 1–59 (1977).
2. Hubener, M., Shoham, D., Grinvald, A. & Bonhoeffer, T. Spatial relationships among three columnar systems in cat area 17. *J. Neurosci.* **17,** 9270–9284 (1997).
3. Swindale, N. V. How many maps are there in visual cortex? *Cereb. Cortex* **10,** 633–643 (2000).
4. Swindale, N. V., Shoham, D., Grinvald, A., Bonhoeffer, T. & Hubener, M. Visual cortex maps are optimized for uniform coverage. *Nature Neurosci.* **3,** 822–826 (2000).
5. Issa, N. P., Trepel, C. & Stryker, M. P. Spatial frequency maps in cat visual cortex. *J. Neurosci.* **20,** 8504–8514 (2000).
6. Everson, R. M., Prashanth, A. K., Gabbay, M., Knight, B. W., Sirovich, L. & Kaplan, E. Representation of spatial frequency and orientation in the visual cortex. *Proc. Natl Acad. Sci. USA* **95,** 8334–8338 (1998).
7. Shmuel, A. & Grinvald, A. Functional organization for direction of motion and its relationship to orientation maps in cat area 18. *J. Neurosci.* **16,** 6945–6964 (1996).
8. Weliky, M., Bosking, W. H. & Fitzpatrick, D. A systematic map of direction preference in primary visual cortex. *Nature* **379,** 725–728 (1996).
9. Bonhoeffer, T. & Grinvald, A. in *Brain Mapping: The Methods* (eds Toga, A. W. & Mazziotta, J. C.) 55–97 (Academic, New York, 1996).
10. Wuerger, S., Shapley, R. & Rubin, N. 'On the visually perceived direction of motion' by Hans Wallach, 60 years later. *Perception* **25,** 1317–1367 (1996).
11. Adelson, E. H. & Movshon, J. A. Phenomenal coherence of moving visual patterns. *Nature* **300,** 523–525 (1982).
12. De Valois, R. L. & De Valois, K. K. *Spatial Vision* (Oxford Univ. Press, New York, 1988).
13. Lorenceau, J., Shiffrar, M., Wells, N. & Castet, E. Different motion sensitive units are involved in recovering the direction of moving lines. *Vision Res.* **33,** 1207–1217 (1993).
14. Pack, C. C. & Born, R. T. Temporal dynamics of a neural solution to the aperture problem in visual area MT of macaque brain. *Nature* **409,** 1040–1042 (2001).
15. Shoham, D., Hubener, M., Schulze, S., Grinvald, A. & Bonhoeffer, T. Spatio-temporal frequency domains and their relation to cytochrome oxidase staining in cat visual cortex. *Nature* **385,** 529–533 (1997).
16. Hubel, D. H. & Wiesel, T. N. Receptive fields and functional architecture in two non-striate visual areas (18 and 19) of the cat. *J. Neurophysiol.* **28,** 229–289 (1965).
17. Gilbert, C. D. Laminar differences in receptive field properties of cells in cat primary visual cortex. *J. Physiol. (Lond.)* **268,** 391–421 (1977).
18. Skottun, B. C., Zhang, J. & Grosof, D. H. On the direction selectivity of cells in the visual cortex to drifting dot patterns. *Vis. Neurosci.* **11,** 885–897 (1994).
19. Movshon, J. A., Thompson, I. D. & Tolhurst, D. J. Spatial summation in the receptive fields of simple cells in the cat's striate cortex. *J. Physiol. (Lond)* **283,** 53–77 (1978).
20. Movshon, J. A., Thompson, I. D. & Tolhurst, D. J. Receptive field organization of complex cells in the cat's striate cortex. *J. Physiol. (Lond.)* **283,** 79–99 (1978).
21. De Valois, K. K., De Valois, R. L. & Yund, E. W. Responses of striate cortex cells to grating and checkerboard patterns. *J. Physiol. (Lond.)* **291,** 483–505 (1979).
22. Gizzi, M. S., Katz, E., Schumer, R. A. & Movshon, J. A. Selectivity for orientation and direction of motion of single neurons in cat striate and extrastriate visual cortex. *J. Neurophysiol.* **63,** 1529–1543 (1990).
23. Hammond, P. & Smith, A. T. Directional tuning interactions between moving oriented and textured stimuli in complex cells of feline striate cortex. *J. Physiol. (Lond.)* **342,** 35–49 (1983).
24. Skottun, B. C., Grosof, G. H. & De Valois, R. L. Responses of simple and complex cells to random dot patterns: a quantitative comparison. *J. Neurophysiol.* **59,** 1719–1735 (1988).
25. Geisler, W. S., Albrecht, D. G., Crane, A. M. & Stern, L. Motion direction signals in the primary visual cortex of cat and monkey. *Vis. Neurosci.* **18,** 501–516 (2001).
26. Galuske, R. A. W., Schmidt, K. E., Kluge, T. & Singer, W. Motion and velocity representation in cat primary visual cortex. *Soc. Neurosci. Abstr.* vol. 27. Program No. 164.2 (2001).
27. Carandini, M., Heeger, D. J. & Movshon, J. A. in *Cerebral Cortex* (ed. Ulinski, P. S.) vol. 13, 401–443 (Kluwer Academic/Plenum, New York, 1999).
28. Adelson, E. H. & Bergen, J. R. Spatiotemporal energy models for the perception of motion. *J. Opt. Soc. Am. A* **2,** 284–299 (1985).
29. White, L. E., Bosking, W. H., Williams, S. M. & Fitzpatrick, D. Maps of central visual space in ferret V1 and V2 lack matching inputs from the two eyes. *J. Neurosci.* **19,** 7089–7099 (1999).

Supplementary Information accompanies the paper on **www.nature.com/nature**.

Acknowledgements We thank D. Purves, J. A. Movshon, S. Nundy, J. C. Crowley and members of the Fitzpatrick laboratory for helpful discussions. This work was supported by a grant from the National Institutes of Health to D.F.

Competing interests statement The authors declare that they have no competing financial interests.

Correspondence and requests for materials should be addressed to D.F. (fitzpat@neuro.duke.edu).

Cyclic AMP/GMP-dependent modulation of Ca^{2+} channels sets the polarity of nerve growth-cone turning

Makoto Nishiyama*, Akemi Hoshino*, Lily Tsai*, John R. Henley†, Yoshio Goshima‡, Marc Tessier-Lavigne§, Mu-ming Poo† & Kyonsoo Hong*

** Department of Biochemistry, New York University School of Medicine, New York, New York 10016-6402, USA*
† Division of Neurobiology, Department of Molecular and Cell Biology, University of California at Berkeley, Berkeley, California 94720-3200, USA
‡ Department of Molecular Pharmacology and Neurobiology, Yokohama City University School of Medicine, Yokohama 236-0004, Japan
§ Howard Hughes Medical Institute, Department of Biological Sciences, Stanford University, Stanford, California 94305-5020, USA

Signalling by intracellular second messengers such as cyclic nucleotides and Ca^{2+} is known to regulate attractive and repulsive guidance of axons by extracellular factors[1,2]. However, the mechanism of interaction among these second messengers in determining the polarity of the guidance response is largely unknown. Here, we report that the ratio of cyclic AMP to cyclic GMP activities sets the polarity of netrin-1-induced axon guidance: high ratios favour attraction, whereas low ratios favour repulsion. Whole-cell recordings of Ca^{2+} currents at *Xenopus* spinal neuron growth cones indicate that cyclic nucleotide signalling directly modulates the activity of L-type Ca^{2+} channels